Numerical and Experimental Study on Nugget Formation in Resistance Spot Welding for High Strength Steel Sheets in Automobile Bodies†

MA Ninshu* and MURAKAWA Hidekazu**

Abstract

Resistance spot welding is the most popular joining process in automobile body assembly production lines. There have been many researches concerned with spot welding for two pieces of sheets. In order to reduce the cost and improve the strength of the lightweight automobile bodies, resistance spot welding for multi-pieces of sheets has to be investigated before production.

In this paper, resistance spot welding for three pieces of high strength steel sheets is mainly taken as an object and the nugget formation process is firstly investigated by experiments. Then the spot welding process is simulated by FEM program JWRIAN developed by the authors with the coupling of the electrical field, thermal field and mechanical field. The nugget size and its formation process predicted by FEM agree very well with experimental results. Based on the simulation results, weldable conditions (current, cycles and force) of spot welding for both two pieces and three pieces of high strength steel sheets can estimated with a good accuracy.

KEY WORDS: (Spot welding), (Welding conditions), (Nugget Formation), (Simulation), (Experiment)

1. Background

Finite Element Method (FEM) has been routinely applied in automobile industries for the analysis of structural strength and component design because of the spread of computers with high performance, low price and development of FEM software. It has also been playing a significant role in predicting the behavior of the weld cracking, weld distortion and residual stress in a welding area[1)].

To assemble various components of automobile bodies, the resistance spot welding process is widely used because of its low cost and high productivity. In order to determine spot welding conditions in production, many experiments have to be performed. Compared with experimental researches, only a few simulation examples for simple two pieces of sheets are reported[2-11)]. This is because the resistance spot welding process is coupling with three physical fields which are the electrical field, the thermal field and the mechanical field.

In this paper, spot welding for three pieces of high strength steel sheets used in lightweight automobile bodies is mainly taken as an object and the nugget formation process were firstly investigated by experiments. FEM program JWRIAN[1-4)] developed by the authors and the visualization option is added recently. Then, the simulations for electric current flow, heat generation and nugget formation in the spot welding process are carried out. By comparing the simulation results with experimental ones, the accuracy of FEM program JWRIAN is verified. Lastly, the weldable conditions (current, cycles and force) of resistance spot welding for three pieces of high strength steel sheets are estimated based on simulation results.

2. Experimental conditions and results

Resistance spot welding conditions include three parameters which are force (axial squeezing force), electric current and current cycles, respectively. The welding conditions for three pieces of high strength steel sheets are shown in **Table 1** which indicates that the tensile strength and thickness of sheets are 270MPa and 0.7mm, 590MPa and 1.4mm, 590MPa and 1.8mm, respectively. Three levels of welding current (5.0kA, 6.0kA, 7.0kA) are selected in experiments. The time of current flow is expressed by current cycles which are widely used in industry whether the direct current or alternative current is selected. One cycle is 0.02sec and direct current is used in this paper. The maximum cycles of welding current are 17 cycles (time is 0.34sec). The axial force applied to electrodes is 250kgf (2450N).

† Received on December 18, 2009
* Guest Associate Professor
** Professor
Transactions of JWRI is published by Joining and Welding Research Institute, Osaka University, Ibaraki, Osaka 567-0047, Japan

Table 1 Spot welding conditions

+Electrode / −Electrode	Test pieces	Current	Cycles	Force
	270C/t0.7 590Y/t1.4 590Y/t1.8	5.0kA 6.0kA 7.0kA	17(340ms) 17(340ms) 17(340ms)	250kgf 250kgf 250kgf

	5.0kA, 17cycles 250kgf	6.0kA, 17cycles 250kgf	7.0kA, 17cycles 250kgf
270C/t0.7 590Y/t1.4 590Y/t1.8	 D=4.99, h=2.53	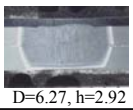 D=6.27, h=2.92	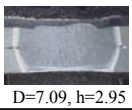 D=7.09, h=2.95

Fig. 1 Measured nugget sizes at different welding currents

Cycle=4(80ms) 7.0kA,250kgf	Cycle=5(100ms) 7.0kA,250kgf	Cycle=7(140ms) 7.0kA,250kgf	Cycle=10(200ms) 7.0kA,250kgf	Cycle=13(260ms) 7.0kA,250kgf	Cycle=17(340ms) 7.0kA,250kgf
Not welded D:Nugget diameter h:Nugget depth	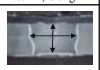 D=3.92, h=2.55	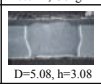 D=5.08, h=3.08	 D=6.12, h=3.25	 D=6.52, h=3.05	 D=7.09, h=2.95

Fig. 2 Nugget sizes measured at different welding cycles

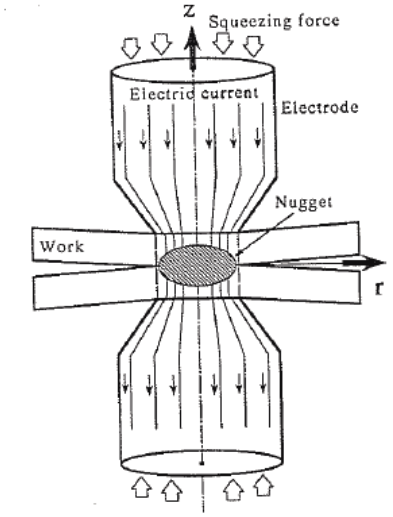

Fig. 3 Schematic showing of resistance spot welding process

The nugget diameter D and depth h measured in experiments with different welding currents are shown in **Fig. 1**. To know the nugget formation processes, the nugget sizes for 7.0kA welding current are measured at the cycles 4, 5, 7, 10, 13, 17, respectively. As shown in **Fig. 2**, the nugget is not generated before the 4-th cycle and nugget sizes increase slightly with increasing of welding time after 5-th cycle.

3. Theories and FEM equations for resistance spot welding process

Figure 3 shows a simple model of spot welding. Current and force applied to the electrodes are electrical load and mechanical load, respectively. As simply described in the above sections, the spot welding process couples electrical field, thermal field and mechanical field during contact.

3.1 Theory and FEM equations of static electrical field

If the effect of magnetic field and its time derivatives are negligibly small, the electrical field can be expressed by electrical potential ϕ satisfying the Laplace equation **Eq. (1)** which is a characteristic of the static electrical field.

$$\varepsilon \frac{1}{r}\frac{\partial}{\partial r}(r\frac{\partial \phi}{\partial r}) + \varepsilon \frac{\partial}{\partial z}(\frac{\partial \phi}{\partial z}) = 0 \qquad (1)$$

Where, ε is the electrical conductivity of the material. The relation between electrical conductivity and electrical resistivity R is given by **Eq. (2)**.

$$\varepsilon = 1/R \qquad (2)$$

The electrical potential can be determined by solving **Eq. (1)** if the electrical boundary conditions are considered. In spot welding, there are two types of boundary conditions which are zero potential boundary condition (BC1) and current boundary condition (BC2) defined by **Eq. (3)** and **Eq. (4)**, respectively.

$$\phi = 0 \text{ for BC1} \qquad (3)$$

$$i = i_0[A/(mm^2 s)] \text{ for BC2} \qquad (4a)$$

$$\int i_0 dS = I_0 \qquad \text{for BC2} \qquad (4b)$$

Where, i_0 is current flux at unit area of surface dS of BC2. The integral of current flux i_0 will be the total welding current I_0. If alternating current is applied in spot welding, the current I should be replaced by $I_0 \cdot \sin(2\pi ft)$ where f is frequency of alternating current.

If electrical potential ϕ and electrical conductivity ε are known, the current density i in x, y z directions and the Joule heat generation per unit volume $\dot{q}_V$ can be calculated by **Eqs. (5)** and **(6)**, respectively.

$$i_r = -\varepsilon \frac{\partial \phi}{\partial r}, \quad i_z = -\varepsilon \frac{\partial \phi}{\partial z} \qquad (5)$$

$$\dot{q}_V[J/(mm^3 s)] = \frac{1}{\varepsilon}(i_r^2 + i_z^2) \qquad (6)$$

When FEM is used to solve the electrical potential $\{\phi\}$ at FEM nodes, the static electrical FEM equation **Eq. (7)** for spot welding can be derived as follows,

$$[K]\{\phi\} = \{\bar{I}\} \qquad (7a)$$

$$\{\phi_{BC1}\} = 0 \ \ for\ BC1 \qquad (7b)$$

Where, [K] is the global electric matrix which is assembled from element electric matrix [K^e] using shape function [N] of element for electrical potential. The components of equivalent nodal current vector $\{\bar{I}\}$ given by **Eq. (7e)** have nonzero value only at the specified nodes (BC2) where welding current is applied

$$\phi(r,z) = \sum N_i(r,z)\phi_i \qquad (7c)$$

$$[K^e] = \int_e \varepsilon(\frac{\partial [N]^T}{\partial r}\frac{\partial [N]}{\partial r} + \frac{\partial [N]^T}{\partial z}\frac{\partial [N]}{\partial z})2\pi r \cdot dr \cdot dz \qquad (7d)$$

$$\{\bar{I}^e\} = \int_{BC_2} i_0[N]dS$$
$$\{\bar{I}\} = \sum_e \{\bar{I}^e\} = \{0,,,0,I_{BC2},0,,,0\}^T \quad (7e)$$

3.2 Theory and FEM equations of thermal field

The thermal field can be described by **Eq. (8)** with various boundary conditions.

$$c\rho\frac{\partial T}{\partial t} = \lambda\frac{1}{r}\frac{\partial}{\partial r}(r\frac{\partial T}{\partial r}) + \lambda\frac{\partial}{\partial z}(\frac{\partial T}{\partial z}) + \dot{q}_V \quad (8)$$

where, $\dot{q}_V$ is the Joule heat generation rate per unit volume and c, ρ, λ are the heat capacity, density and thermal conductivity of the materials.

There are three types of thermal boundaries, temperature boundary (BC1), heat flux boundary (BC2) and heat convection boundary (BC3) defined by **Eq. (9)**, **Eq. (10)** and **Eq. (11)**, respectively.

$$T = T_{BC1} \quad \text{at BC1} \quad (9)$$
$$\dot{q} = \dot{q}_A[J/(mm^2 s)] \quad \text{at BC2} \quad (10)$$
$$\dot{q} = \beta(T_{BC3} - T_0) \quad \text{at BC3} \quad (11)$$

where $T_{BC1}, \dot{q}_A, \beta, T_{BC3}, T_0$ are the given temperature at BC1, heat flux at BC2, heat transfer coefficient for both convection and radiation boundary, temperature at BC3 and temperature of the surrounding air, respectively.

If FEM is used to describe the thermal conduction and heat transfer boundary defined by **Eqs. (8)-(11)**, transient temperature $\{T\}$ and its rate $\{\frac{\partial T}{\partial t}\}$ at all nodes can be given by **Eq. (12)**.

$$[C]\left\{\frac{\partial T}{\partial t}\right\} + [K]\{T\} = \{Q\} \quad (12)$$

where, [K], [C] and {Q} are the thermal conductivity matrix, heat capacity matrix and equivalent nodal heat, respectively. The element value of [K], [C] and {Q} are given by **Eqs. (13a)**, **(13b)** and **(13c)**, respectively.

$$[K^e] = \int_e \lambda(\frac{\partial[N]^T}{\partial r}\frac{\partial[N]}{\partial r} + \frac{\partial[N]^T}{\partial z}\frac{\partial[N]}{\partial z})2\pi r\cdot dr\cdot dz + \int_{BC3}\beta[N][][N]dS \quad (13a)$$

$$[C^e] = \int_e c\rho[N]^T[N]2\pi r\cdot dr\cdot dz \quad (13b)$$

$$\{Q^e\} = \int_e \dot{q}_V[N]^T dV + \int_{BC2}\dot{q}_0[N]^T dS + \int_{BC3}\beta T_0[N]^T dS \quad (13c)$$

The $\dot{q}_V$ in **Eq. (13c)** is the internal Joule heat generation which is given by **Eq. (6)**.

If the temperature rate $\frac{\partial T}{\partial t}$ is defined by **Eq. (14)** based on the Crank-Nicolson method, the temperature $\{T\}$ at time $t + dt$ can be calculated by **Eq. (15)**.

$$\{\frac{\partial T}{\partial t}\} = \frac{\{T\}_{t+dt} - \{T\}_t}{2dt} \quad (14)$$

$$\left(\frac{1}{2}[K] + \frac{[C]}{\Delta t}\right)\{T\}_{t+dt} = \frac{1}{2}(\{Q\}_{t+dt} + \{Q\}_t) + \left(\frac{[C]}{\Delta t} - \frac{1}{2}[K]\right)\{T\}_t \quad (15)$$

3.3 Theory and FEM equations for mechanical filed

The mechanical field is expressed by displacement at FEM nodes and can be obtained by solving elastic plastic FEM equation **Eq. (16)** which was described in detail in reference[1, 12].

$$[K]\{\Delta u\} = \{\Delta F\} + \{R\} \quad (16)$$

Where, $[K], \{\Delta u\}, \{\Delta F\}, \{R\}$ are the stiffness matrix, vector of nodal displacement, vector of equivalent nodal force and vector of residual nodal force, respectively. The element value of $[K], \{\Delta F\}, \{R\}$ is given by **Eqs. (17a)**, **(17b)** and **(17c)**, respectively.

$$[K^e] = \int [B]^T[D^{ep}]\{B\}2\pi r\cdot dr\cdot dz \quad (17a)$$
$$\{\Delta F^e\} = \int [B]^T[D^{ep}]\{\Delta\varepsilon^T\}2\pi r\cdot dr\cdot dz \quad (17b)$$
$$\{R^e\} = \{F\} - \int [B]^T\{\sigma\}2\pi r\cdot dr\cdot dz \quad (17c)$$

The stress $\{\sigma\}$ can be computed by **Eq. (18)** based on thermal elastic plastic theory.

$$\{\sigma\}_{t+dt} = \{\sigma\}_t + \{\Delta\sigma\} \quad (18a)$$
$$\{\Delta\sigma\} = [D^e](\{\Delta\varepsilon\} - \{\Delta\varepsilon^T\} - \{\Delta\varepsilon^p\}) \quad (18b)$$

where, $[D^e]$: Elastic matrix

$[D^{ep}]$: Elastic-plastic matrix

$\{\Delta\sigma\}$: Stress increment

$\{\Delta\varepsilon\}$: Total strain increment

$\{\Delta\varepsilon^T\}$: Thermal strain increment considering the change of Young's modulus and yield stress with temperature

$\{\Delta\varepsilon^p\}$: Plastic strain increment

3.4 Electrical-thermal-mechanical contact model

The contact between an electrode and a sheet or between two sheets is modeled by an interface element[12] as shown in **Fig. 4**.

If the strain ε_n of the interface element in the normal direction n of the contact interface is larger than -0.99, the state of the interface is the non-contact state. In the initial state and non-contact state, the electrical conductivity ε, thermal conductivity λ and Young's modulus E will be zero. This means that current flow

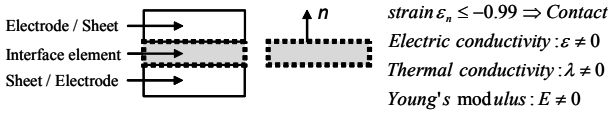

Fig. 4 Interface element for contact

through the interface element and heat generation will be zero at the interface element.If the strain ε_n of the interface element in the normal direction n of the contact interface is equal to or less than -0.99, the state of the interface is the in-contact state. In the contact state, the electrical conductivity ε, thermal conductivity λ and Young's modulus E will be a given value. This means that current flows through the interface element and heat is generated at the interface element. In the contact state, the interface element has a strong stiffness.

3.5 Simulation procedure for resistance spot welding process

The simulation procedure for resistance spot welding process is shown in **Fig. 5**. At the first step, initial contact areas between electrode and a sheet or between two sheets are predicted when force is applied to the electrode using elastic plastic FEM solver for mechanical analysis. Then the current flowing through the contact areas can be computed using electrical FEM solver described in section 3.1. When current density is obtained and Joule heat generation is known, temperature distribution can be computed by thermal FEM solver described in section 3.2. The deformation of welding sheets and electrodes can be simulated by thermal elastic plastic FEM solver described in section 3.3. Lastly, the new contact state is predicted for the next time step as described in section 3.4. This simulation flow is repeated for every time step.

4. FEM simulation conditions

Spot welding is assumed to be an symmetric problem in this paper. **Figure 6** shows the geometry and the mesh division. The minimum mesh size is about 0.2mm.

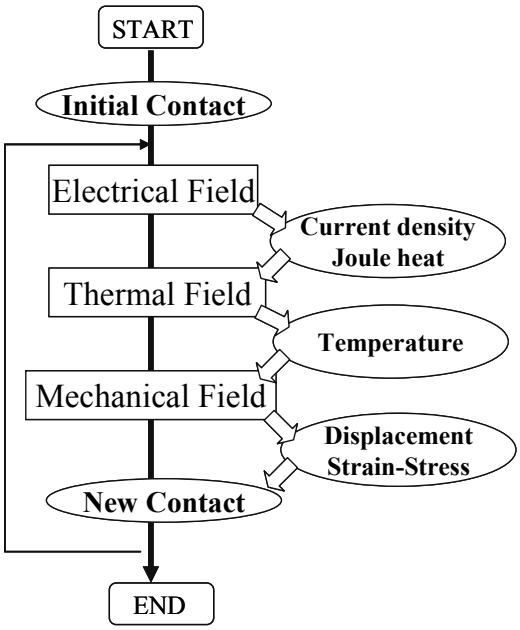

Fig. 5 Simulation flow for spot welding process

The current flows from the upper electrode and zero potential is applied to the boundary of the lower electrode shown in **Fig. 6(a)**. The electrical resistivity R of steel sheets 270C and 590Y is shown in **Fig. 7**. Thermal conductivity λ, heat capacity c and heat transfer coefficient β for heat conduction analysis are shown in **Fig. 8**. The mechanical properties Young's modulus E, Yield stress σ_Y, Poisson's ratio υ, linear plastic hardening coefficient H' and thermal expansion coefficient α of steel sheets used in thermal elastic plastic analysis are shown in **Fig. 9**. The change of material properties with temperature is considered in the three field coupled simulation.

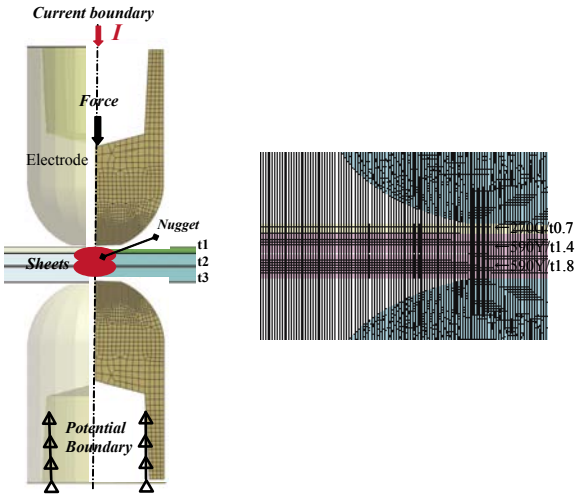

(a) Full model (b) Detail mesh

Fig. 6 FEM model for spot welding process

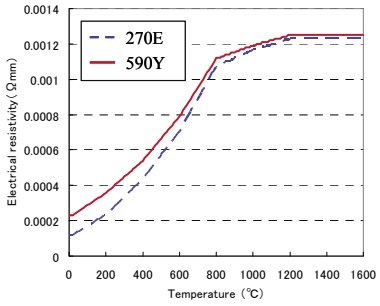

Fig. 7 Electrical resistivity and temperature dependence

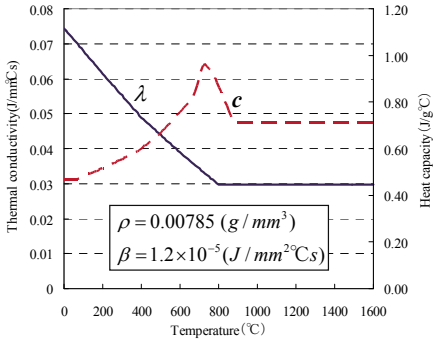

Fig. 8 Thermal properties and temperature dependence

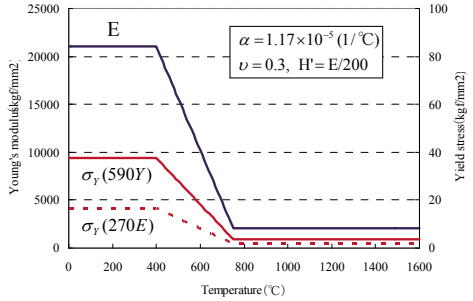

Fig. 9 Mechanical properties and temperature dependence

Table 2 Material properties of electrodes (Cu)

ρ (g/mm3)	R(Ω)	λ (J/mm*℃*s)	
0.0089	1.2E-04	0.314	
c(J/g*℃)	E(kg/mm2)	υ	α (1/℃)
0.389	13000	0.348	1.77E-05

The density ρ , electrical resistivity R, thermal conductivity λ , heat capacity c and Young's modulus E , Poisson's ratio υ of electrode material (Cu) used in electrical-thermal-mechanical simulation are shown in **Table.2**.

A constant nodal current (welding current I_0) is applied to one node at the top position of the upper electrode and a constant nodal force (axial squeezing force) is applied to the top surface of the upper electrode. The potential and displacement at the lower electrode marked by △ in **Fig. 6(a)** are set to zero in the static electrical field simulation and deformation simulation, respectively.

5. Results computed by FEM

The computed current density and its distribution at the 17-th current cycle of spot welding for three pieces of sheets are shown by **Fig. 10**. The current density concentrates at the shape changing corners. The nugget shape and sizes (diameter D and depth h) which are defined by melting temperature (1530℃) at different welding current are shown by **Fig. 11**. With the increase of welding current, nugget sizes increase. **Figure 12** shows the nugget formation process during spot welding. The nugget forms from the 5th cycle when welding current is 7.0kA. Diameter D of nugget increases with the increase of welding current cycles. The number of welding current cycles has a less effect on nugget depth h.

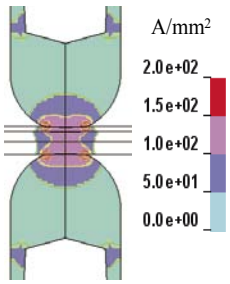

Fig. 10 Computed current density

	5.0kA, 17cycles 250kgf	6.0kA, 17cycles 250kgf	7.0kA, 17cycles 250kgf
270C/t0.7 590Y/t1.4 590Y/t1.8	D=4.90, h=3.12	D=5.80, h=3.60	D=6.40, h=3.75

Fig. 11 Computed Nugget shape and sizes at different welding current

Cycle=4(80ms) 7.0kA,250kgf	Cycle=5(100ms) 7.0kA,250kgf	Cycle=7(140ms) 7.0kA,250kgf	Cycle=10(200ms) 7.0kA,250kgf	Cycle=13(260ms) 7.0kA,250kgf	Cycle=17(340ms) 7.0kA,250kgf
Not welded D:Nugget diameter h:Nugget depth	D=4.04, h=3.35	D=4.98, h=3.60	D=5.52, h=3.70	D=5.97, h=3.80	D=6.39, h=3.75

Fig. 12 Computed nugget sizes during spot welding process

6. Comparison between computed and measured results

Figure 13 shows the changes of nugget sizes with welding current cycles computed by FEM (FEM) and measured by experiment (exp) when the current is 7.0kA and the force is 250kgf. Lines in **Fig. 13** are simulation results by FEM and marks ●, □ are the results measured by experiments. The nugget is not generated before the 4th cycle. The nugget forms initially from the 5 cycle which is called the nugget formation cycle in this paper for easy description. The diameter of the nugget increases with welding cycles after the nugget formation cycle. The depth of nugget keeps almost the same value after the 5th cycle. The nugget formation cycle, diameter and depth of nugget computed by FEM agree very well with the results measured by experiments.

Figure 14 shows the changes of nugget diameter with welding current cycles when welding current is 7.0kA, 6.0kA and 5.0kA, respectively. The marks ○, △, □ are the measured results respectively. The nugget formation cycle for these three current levels is the 5th cycle, the 7th cycle and the 12th cycle, respectively. The nugget diameters predicted by FEM at these three current levels have a good agreement with those measured by experiments.

Using the simulation results, the possible welding zone defined can be predicted according to the welding current and current cycles shown in **Fig. 15**. With the increase of welding current, the nugget formation cycles decrease.

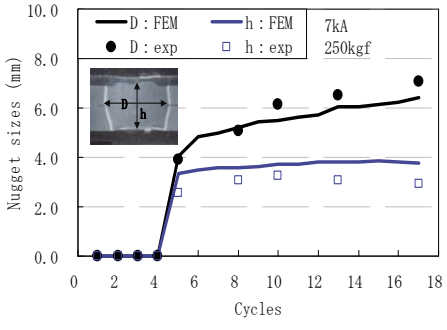

Fig. 13 Nugget formation process

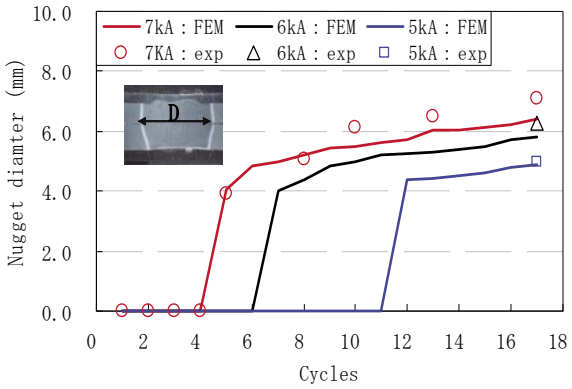

Fig. 14 Welding current vs. nugget formation

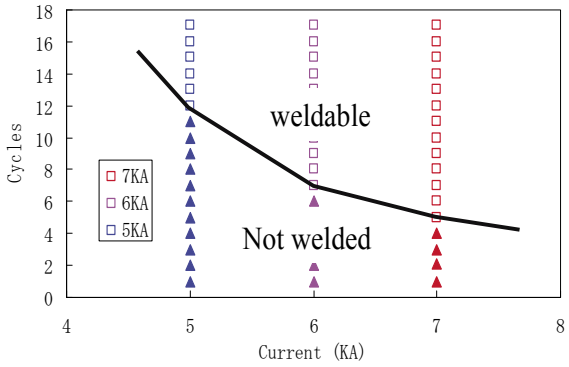

Fig. 15 Weldable conditions for three pieces of sheets

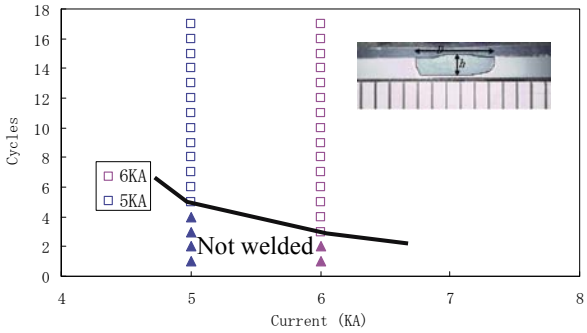

Fig. 16 Weldable conditions for three pieces of sheets

The possible welding conditions of spot welding for traditional two pieces of sheets which predicted by FEM is also shown by **Fig. 16**. The nugget formation cycles for two pieces of sheets are less than the cycles for three pieces of sheets.

7. Conclusions

1) The nugget sizes of resistance spot welding for three pieces of high strength steel sheets are measured by experiments with different welding currents and different welding current cycles.
2) Nugget formation process is simulated with a good accuracy for various spot welding conditions.
3) Minimum welding current cycles for nugget formation and weldable conditions can be accurately predicted by FEM simulation.

Reference

1) Y.Ueda, H.Murakawa and N.Ma : Computational Approach to Welding Deformation and Residual Stresses (in Japanese), Sanpo-pub, Oct. 2007, ISBN 978-4-88318-033-2
2) H.Murakawa, H.Kimura and Y. Ueda: Weldability analysis of spot welding on Aluminum using FEM, Trans of JWRI, Vol24 (1995) No.1, Mathematic modeling of weld phenomena 3 (1997), Edited by H. Cerjack, p.944-966, ISBN 1-86125-010-X.
3) J. Zhang and H. Murakawa : FEM Simulation of the Spot Welding Process (Report-2), Effect of Initial Gap and Electrode-type on Nugget Formation and Expulsion, Trans. JWRI. Vol.27, No.2, 1998, p73-79
4) H. Murakawa, J. X.Zhang and H. Minami: FEM Simulation of the Spot Welding Process (Report-3), Control of WeldingCurrent Using Electrode Displacement for Formation of Large Enough Nugget without Expulsion, Trans. JWRI. Vol.28, No.1, 1999, p41-46
5) K.Matsuyama: Simulation Techniques in Resistance Spot Welding, Journal of the Japan Welding Society, Vol.70 (2001) No.5
6) A.Chakalev: Evaluation for the thermal state of the Metal in Spot welding with the help of the computer, Welding production, Vol.20(1973)No.10
7) U.Dilthey and P.Ohse: The Front Line in Modeling of Resistance Welding, Journal of the Japan Welding Society, Vol.76 (2007) No.2
8) H.A.Nied: The Finite Element Modelling of the Resistance Spot Welding Process, Welding Research Supplement, Vol.63 (1984) No.4
9) W.Zhang: Recent advances and Improvements in simulation if resistance welding processes, Eelding in the world, Vol.50 (2006)
10) J.Khan et al: Numerical Simulation of resistance spot welding process, Numerical heat transfer, part A, Vol.37 (2000)
11) A.De et al: Numerical modelling of resistance spot welding of aluminum alloy, ISIJ international, Vol.43 (2003) No.2
12) Y. Ueda and T. Yamakawa: Analysis of Thermal Elastic-Plastic Stress and Strain during Welding by Finite Element Method, Trans. of Japan Welding Society, Vol.2 (1971) No.2